https://doi.org/10.5194/egusphere-2026-6315
Preprint. Discussion started: 4 November 2026
© Author(s) 2026. CC BY 4.0 License.

Recognizing post-entrapment alteration for robust speleothem fluid inclusion microthermometry

Yuri V. Dublyansky[1]

[1]Institute of Geology, University of Innsbruck, Innsbruck, 6020, Austria

Correspondence to: Yuri V. Dublyansky (yuri.dublyansky@uibk.ac.at)

Abstract. Nucleation-assisted fluid inclusion microthermometry (NA-FIM) provides direct estimates of speleothem formation temperatures (T_{form}), derived statistically from measured homogenization temperatures (T_h). Accurate analysis requires inclusions to act as closed, isochoric systems. However, inclusions frequently undergo post-entrapment alteration via three mechanisms: mechanical stress during preparation, thermal re-equilibration, and direct laser impact during analysis. While severe alteration produces visually obvious leakage, cryptic alteration irreversibly expands inclusion volumes without visual evidence. This expansion systematically lowers fluid density, causing initially symmetrical T_h distributions to distort into asymmetric, right-skewed ones. Consequently, traditional statistical metrics (the mean, median, standard deviation, and standard error) become mathematically untenable and systematically overestimate formation temperatures.

To robustly estimate T_{form} from positively biased data, we propose uniformly applying the first quartile (Q1) of the measured T_h distribution. Numerical simulations demonstrate that Q1 closely approximates the true pristine mean under variable right-skew conditions. To accurately capture uncertainty without relying on parametric assumptions, we recommend reporting overall data scatter using the interquartile range (IQR) and quantifying the precision of the Q1 estimate via bootstrap 95% confidence intervals. This robust approach safeguards the integrity of paleotemperature reconstructions.

1 Introduction

"Classical" Fluid Inclusion Microthermometry (FIM) is applied to inclusions in which a shrinkage bubble has spontaneously formed upon cooling from the formation temperature to room temperature. However, in minerals formed at temperatures below approximately 50°C, spontaneous nucleation is thermodynamically suppressed (Roedder, 1984; Goldstein and Reynolds, 1994). In such cases, the shrinkage bubble fails to form, and the water within the inclusion remains in a metastable, “stretched” state. Consequently, while measurements of homogenization temperatures below ~40°C have occasionally been documented (Wilson et al., 2003; Dublyansky et al., 2001), spontaneous bubble nucleation becomes exponentially less frequent at lower temperatures, severely limiting the practical application of the classical FIM method.

Nucleation-Assisted Fluid Inclusion Microthermometry (NA-FIM) overcomes this metastability by triggering nucleation with short laser pulses (Krüger et al., 2007). The compression waves created by the laser pulse facilitate the formation of a shrinkage

https://doi.org/10.5194/egusphere-2026-6315
Preprint. Discussion started: 4 November 2026
© Author(s) 2026. CC BY 4.0 License.

bubble. Subsequently, the sample is heated in the heating-freezing stage until the bubble disappears, yielding the raw, uncorrected value termed the 'observed homogenization temperature', or $T_{h(obs)}$.

The values of $T_{h(obs)}$ are influenced by the inclusion size and the corresponding volume of the generated bubble due to surface tension effects. Therefore, to determine the actual formation temperature, a Laplace pressure correction (Marti et al., 2012) must be applied to $T_{h(obs)}$ to calculate the size-independent, corrected homogenization temperature $T_{h\infty}$. In this paper, to maintain a streamlined narrative, this Laplace-corrected temperature ($T_{h\infty}$) is hereafter referred to simply as T_h.

NA-FIM is currently the only analytical method capable of providing direct data on the formation temperature (T_{form}) of speleothems, which reflects past environmental temperatures in caves. Because temperatures in the deep interior of caves remain highly stable and closely track the external mean annual air temperature (e.g., Domínguez-Villar et al., 2014), NA-FIM is an exceptionally important tool for paleoclimate reconstruction.

To determine the cave paleotemperatures at the time of fluid entrapment, multiple T_h values must be systematically measured from individual speleothem growth bands. In this context, these discrete growth bands serve as the functional equivalent of a Fluid Inclusion Assemblage (FIA) in classical microthermometry—a petrographically distinct group of coeval inclusions that can reasonably be assumed to have formed synchronously (Goldstein and Reynolds, 1994). T_{form} is derived statistically from the distributions of acquired T_h values, though methodologies vary. In studies where T_h values yield near-Gaussian distributions, the mean value is the preferred estimator (Krüger et al., 2025). This assumed normality justifies the use of the standard deviation (SD) and the standard error of the mean (SE) as estimators of uncertainty (Meckler et al., 2015; Løland et al., 2022; Maccali et al., 2023; Pahl et al., 2025).

Crucially, many reported datasets contain, in addition to a normally distributed component, varying proportions of inclusions that homogenize at significantly higher temperatures. These are interpreted as altered inclusions whose density has changed post-entrapment. Such datasets are typically filtered using a twofold procedure: (1) the application of a cut-off temperature to exclude T_h values considered unrealistically high for the specific cave environment (e.g., Meckler et al., 2015; Løland et al., 2022); and (2) the exclusion of statistical outliers based on formal criteria, such as the 3SD rule (Løland et al., 2022) or four times the Median Absolute Deviation (Krüger et al., 2025).

In contrast, in a study of a stalagmite from Milandre Cave, Switzerland, Spadin et al. (2015) observed distinctly right-skewed, non-Gaussian T_h distributions. By comparing T_h from recently deposited calcite (the last 470 years) with reconstructed surface temperatures and instrumental cave temperature data, the authors concluded that only the lowest 30% of the data reflected the true formation temperature. In the Milandre dataset, applying Gaussian metrics would result in a significant and unrealistic overestimation of T_{form}. Consequently, the authors recommended relying exclusively on the lowest acquired T_h values to reconstruct formation temperatures.

To date, the study by Spadin et al. (2015) represents the only published record reconstructing paleotemperatures from an obviously and severely altered population of speleothem fluid inclusions. We anticipate that as the NA-FIM method becomes more widely adopted, the number of such non-ideal datasets will grow. This paper evaluates the most effective strategies for

https://doi.org/10.5194/egusphere-2026-6315
Preprint. Discussion started: 4 November 2026
© Author(s) 2026. CC BY 4.0 License.

extracting reliable paleotemperature records from speleothems whose fluid inclusion assemblages have undergone substantial post-entrapment alteration.

2 Reconstructing formation temperatures from altered inclusions: Proposed approach

Post-entrapment alteration of fluid inclusions is virtually always associated with the expansion of inclusion volumes and a corresponding decrease in the density of the trapped water, which drives measured T_h values upward. Consequently, alteration presents a strictly unidirectional positive error vector; samples that have experienced appreciable alteration are expected to exhibit asymmetric, right-skewed distributions.

For samples whose inclusions have experienced negligible post-entrapment alteration (demonstrating tight, symmetrical T_h distributions), equating T_{form} to the arithmetic mean is the most straightforward and scientifically defensible approach. In contrast, for altered distributions, traditional parametric metrics, such as the arithmetic mean and the median, become mathematically compromised and systematically overestimate the true entrapment temperature. This fundamental dichotomy raises two practical questions: (1) which metrics should be used when reconstructing T_{form} from altered inclusion populations, and (2) should different metrics be applied to pristine versus altered samples?

2.1 Evaluating statistical metrics for altered fluid inclusion populations

From physical considerations, the unaltered fraction of a fluid inclusion population must be represented by the lowest consistent values within the T_h distribution. Rather than relying on a fixed, arbitrary percentage of the lowest data points (e.g., Spadin et al., 2015), we propose estimating the true formation temperature from fluid inclusion data variably affected by positive bias (stretching or re-equilibration) using the first quartile (Q1, the 25th percentile) of the measured T_h distribution, instead of the arithmetic mean or median. This choice is motivated by the following considerations.

First, in the absence of bias, a pristine distribution is well-characterized by its mean, but the presence of a variable positive bias shifts both the mean and the median rightward and away from the true value.

Second, Q1 is highly resistant to extreme positive outliers and relies strictly on the lower tail of the distribution, where inclusions are least affected by post-entrapment alteration.

Third, standard practice of NA-FIM commonly involves user-defined data cutoffs (such as maximum temperature thresholds based on regional climate constraints). Q1 offers a critical advantage over the mean or percentage-trimmed means because its numerical value remains unchanged by the specific placement of these cutoffs, provided they lie above the 25th percentile.

Fourth, while Q1 slightly underestimates the true mean in a perfectly symmetric, unbiased distribution (by approximately 0.67 standard deviations), this offset is small, quantifiable, and directionally conservative. Under conditions of variable positive bias, numerical simulation experiments (detailed in subsequent sections) demonstrate that Q1 provides a much closer approximation to the true pristine mean than either the median or the arithmetic mean.

https://doi.org/10.5194/egusphere-2026-6315
Preprint. Discussion started: 4 November 2026
© Author(s) 2026. CC BY 4.0 License.

An important caveat must be noted. In samples where fluid inclusions have experienced only partial alteration (meaning a subset of inclusions remains pristine), Q1 closely approaches the true trapping temperature. However, in samples where the entire population carries some degree of positive bias, the absolute magnitude of this baseline shift cannot be assessed from microthermometric data alone; and an external bias correction is required. Consequently, for heavily altered samples, Q1 represents a conservative upper bound for T_{form}. Recognizing strongly altered populations is therefore a vital analytical task.

2.2 Uniform versus conditional application of statistical metrics

As established, the arithmetic mean and the median are appropriate estimators for ideal, Gaussian distributions, whereas the first quartile (Q1) is preferable for right-skewed, altered distributions. This raises an obvious methodological question: should researchers evaluate the shape of each acquired T_h distribution and conditionally switch between these metrics? Before addressing this, we must first consider a major operational constraint in NA-FIM, which is the limited number of discrete measurements obtainable from a typical inclusion assemblage.

In published studies, the number of T_h values obtained per individual speleothem growth band varies widely depending on sample quality. While high-quality material can yield 40 to 60 measurements (Løland et al., 2022; Pahl et al., 2025; Krüger et al., 2025), challenging samples with a low abundance of usable inclusions may average only 10 to 14 measurements (Spadin et al., 2015; Maccali et al., 2023; Koltai et al., 2024).

At sample sizes between 20 and 40, formal normality tests (such as the Shapiro–Wilk test) exhibit low statistical power. Consequently, they frequently fail to detect even substantial departures from normality, leading to false confidence in an assumed normal distribution. Because of this limitation, the normality or alteration-induced asymmetry of a dataset in practical NA-FIM workflows is typically diagnosed via visual inspection, an approach that is inherently subjective.

Four operational strategies can be considered for reconstructing T_{form} from T_h distributions:

1. **Use the mean for visually symmetric samples and Q1 for visibly skewed ones**: This approach is methodologically inconsistent, relies on subjective investigator decisions, and cannot be systematically replicated.
2. **Test normality formally and switch between the mean and Q1 based on a threshold p-value:** This method is unreliable because formal tests lack the statistical power to resolve distributions at typical sample sizes (n = 20 to 40), rendering the resulting p-values largely inconclusive.
3. **Use the arithmetic mean uniformly for all distributions**: This strategy introduces unquantifiable positive errors if any sample within the time series has undergone post-entrapment alteration.
4. **Use Q1 uniformly for all distributions**: This approach consistently applies a single mathematical operator across the entire dataset, though it slightly underestimates T_{form} when a distribution is truly pristine.

We consider Option 4, the uniform use of Q1, to be the most scientifically defensible method for paleoclimate reconstructions. It provides four distinct analytical benefits:

- **Objectivity:** It eliminates subjective, user-dependent decisions regarding which samples are "biased enough" to warrant alternative treatment.

https://doi.org/10.5194/egusphere-2026-6315
Preprint. Discussion started: 4 November 2026
© Author(s) 2026. CC BY 4.0 License.

- **Comparability:** All samples across a time series are treated identically; time-series variations therefore reflect true environmental signals rather than artifacts of switching statistical methods.
- **Predictable bias:** Q1 underestimates T_{form} for perfectly normal samples by a stable, known offset (approximately 0.67 standard deviations). This represents a consistent, quantifiable, and directionally conservative trade-off.
- **Robustness:** The reliability of Q1 is independent of the presence, absence, or intensity of positive alteration tails.

Ultimately, by adopting a uniform Q1 approach, we accept a small, known, and directionally conservative error in pristine samples to safeguard the dataset against large, unquantifiable, and non-conservative overestimations in altered samples.

2.3 Quantifying statistical uncertainty in altered populations

To parallel the use of traditional parametric statistics, where the standard deviation (SD) and standard error of the mean (SE) characterize a normal distribution, we define two distinct metrics to accompany Q1-based T_{form} estimates. Overall data scatter within a growth band should be reported using the interquartile range (IQR). Meanwhile, the statistical uncertainty of the Q1 estimate itself (representing the precision of the calculated T_{form}) is quantified via bootstrap 95% confidence intervals (95% CI). These intervals are determined using the percentile method with a recommended minimum of 2,000 bootstrap resamples, isolating the central 95% of the resulting empirical distribution to ensure numerical stability. These 95% CI values should then be utilized in graphical data presentations, such as time series plotting sample age against the respective Q1 temperature estimates.

3 Mechanisms of post-entrapment alteration of fluid inclusions in speleothems

Speleothems are typically composed of calcite, a relatively soft mineral with perfect cleavage, and possess highly variable fabrics (Frisia et al., 2000). Within speleothems, fluid inclusions may reside either within individual crystals or domains (intra-crystalline), or along boundaries between adjacent crystals (inter-crystalline). Because they are hosted by such structurally heterogeneous media, fluid inclusions in speleothems are particularly prone to post-entrapment alteration via stretching, partial opening, or leakage.

We distinguish three primary drivers of inclusion alteration relevant for NA-FIM:

1. **Mechanical:** stress-induced deformation;
2. **Thermal:** exposure to elevated temperatures relative to the formation temperature;
3. **Laser-induced:** alteration occurring directly during the NA-FIM analytical sequence.

Mechanical alteration occurs prior to analysis during sample handling and preparation. Thermal alteration affects speleothems formed in relatively low-temperature caves that are subsequently exposed to warmer ambient temperatures during transportation, storage, sample preparation, and analysis. Finally, laser-induced alteration occurs directly during the acquisition of paleotemperature data. Although these alteration processes have distinct physical origins and affect inclusions differently,

https://doi.org/10.5194/egusphere-2026-6315
Preprint. Discussion started: 4 November 2026
© Author(s) 2026. CC BY 4.0 License.

they share a common consequence: the inclusion volume increases, and the density of the enclosed water correspondingly decreases. Consequently, such inclusions yield T_h values that are systematically higher than the true formation temperature.

The magnitude of induced alteration (encompassing both the degree to which individual inclusions are altered and the proportion of affected inclusions within a sample) is highly sample-specific. It depends on three main factors: (i) the character and intensity of the alteration, (ii) the size and shape of the inclusions, and (iii) the speleothem fabric. Strong alteration may lead to significant changes in inclusion volume, partial opening, or fluid leakage. Large vapor bubbles appearing in such inclusions make them easily recognizable and clearly unsuitable for NA-FIM. In contrast, when alteration is cryptic, the affected inclusions may show no visual evidence of volume change and remain in a single-phase liquid state.

In the following sections, we provide a physics-informed evaluation of the three alteration mechanisms along with their diagnostic statistical signatures in NA-FIM analysis. These signatures are examined graphically using stacked T_h histograms partitioned by inclusion size class, as well as cross-plots of inclusion volume versus T_h. This volume-temperature cross-plot format is natively implemented in the custom MATLAB software utilized by the Fluid Inclusion Laboratory within the Department of Earth Sciences at the University of Bergen, Norway (Pasqualetto et all., in preparation), which is currently the sole facility globally where NA-FIM data acquisition is conducted.

As a baseline, we assume that in an unaltered, pristine speleothem lamina, the homogenization temperatures of fluid inclusions exhibit a symmetrical, narrow Gaussian distribution centered around the true ambient cave temperature. When subjected to alteration, this pristine distribution breaks down. We model how specific alteration drivers modify these statistical distributions, illustrating distinct scenarios with simulated populations, and conclude by providing mitigation strategies to isolate pristine T_h values. To facilitate interactive exploration of these dynamics, the corresponding physics-informed simulation tools and source code are provided as an open-access modeling suite (Dublyansky, 2026a). To evaluate these alteration modes, we employ a simulation setup based on a baseline formation temperature of 15°C, representative of mid-latitude cave environments. Alteration is modeled across three distinct volume-dependent classes: V1 (< 1,000 µm³), V2 (1,000 to 10,000 µm³), and V3 (10,000 to 100,000 µm³). These classes encompass the majority of the volumetric spectrum reported in recent literature (e.g., Meckler et al., 2015; Løland et al., 2022; Maccali et al., 2023; Pahl et al., 2025; Krüger et al., 2025), ensuring the simulations represent typical speleothem fluid inclusion populations.

Note that the outcomes presented below are based on a simulated population of 100 inclusions. This size was selected to ensure statistical representativeness and graphical clarity, whereas practical NA-FIM studies typically yield 20 to 40 measurements. Because empirical datasets effectively subsample from this broader distribution, real-world distributions will appear less visually pronounced and will display higher stochastic scatter. These synthetic outcomes are therefore designed to illustrate underlying alteration mechanisms and guide data interpretation, rather than act as rigid visual templates for experimental results.

https://doi.org/10.5194/egusphere-2026-6315
Preprint. Discussion started: 4 November 2026
© Author(s) 2026. CC BY 4.0 License.

4 Mechanical Alteration

The preparation of 300-µm-thick sections required for NA-FIM analysis involves inevitable mechanical loading during sample wafering with precision diamond-wire or low-speed rotary saws (≤ 300 RPM). While low-speed cutting accompanied by continuous water cooling minimizes thermal friction and high-frequency vibrations, the physical interaction between the cutting medium and the calcite host still poses a distinct risk to fluid inclusion integrity. Given the low hardness, perfect cleavage, and structurally complex fabrics of speleothem calcite, the primary analytical threat during sample preparation is not obvious inclusion opening and total fluid loss, but rather cryptic stretching. This subtle, irreversible volume increase remains visually undetectable under standard optical microscopy yet systematically shifts T_h values toward artificially higher temperatures.

4.1 Stress concentration as a function of inclusion geometry

Fluid inclusions act as internal stress concentrators within the mineral lattice. When an external cutting blade or abrasive grit exerts a mechanical load on the sample, the localized stress at the inclusion-host interface is magnified. The stress concentration factor (K_t) is highly sensitive to the inclusion's shape, aspect ratio, and orientation relative to the applied force, and can be conceptually expressed via the relationship:

$$K_t = 1 + 2\sqrt{\frac{L}{r}} \quad \text{(Eq. 1)}$$

where L represents the characteristic length of the fluid inclusion cavity along the axis of stress, and r is the radius of curvature at its narrowest point. The endmembers of this geometric continuum correspond closely to our established volume classes:

- **V1 inclusions (< 1,000 µm³):** Smaller inclusions tend toward equant, compact geometries and are predominantly intra-crystalline. This configuration results in relatively low K_t values and a generally uniform distribution of the mechanical load across the inclusion wall.
- **V3 inclusions (10,000 to 100,000 µm³):** In large volume ranges, speleothem fluid inclusions are frequently elongated or highly irregular. They are also more likely to occupy inter-crystalline positions along crystal boundaries. These complex geometries yield significantly elevated K_t values, particularly at sharp vertices or elongated "tails" which act as ideal initiation sites for micro-fractures or dislocation propagation along calcite cleavage planes.

4.2 Obvious failure vs. cryptic stretching

In practical microthermometry, fluid inclusions that undergo catastrophic failure (such as total or partial leakage via micro-fractures intersecting the surface of the thick section) do not pose a risk to data accuracy. These failed systems are easily recognized and filtered out prior to analysis using two distinct diagnostic criteria: (a) the initial presence of an anomalously large vapor phase at room temperature or the complete lack of a liquid water phase; and (b) the sudden, explosive expansion

https://doi.org/10.5194/egusphere-2026-6315
Preprint. Discussion started: 4 November 2026
© Author(s) 2026. CC BY 4.0 License.

of a large vapor bubble upon initial laser impact. Consequently, such inclusions are immediately rejected during optical screening and analysis.

The far greater danger to paleoclimate reconstructions lies in cryptic stretching. In larger fluid inclusions, the mechanical energy transferred during the cutting and grinding process may be insufficient to cause macroscopic fracturing but high enough to induce a minute volume expansion via the incipient unzipping of cleavage planes or micro-plastic dislocation glide. This volume change cannot be recognized via optical petrography yet is large enough to induce a positive error in the resulting T_h values. Because these cryptically stretched inclusions appear perfectly pristine and successfully maintain their metastable, liquid-only state until laser-induced bubble nucleation occurs, they are easily accepted by the operator as representative of the original cave environment.

4.3 Proximity to the cut surface

The dimensions of the thick section (typically around 300 μm in thickness) introduce a strong spatial control on the vulnerability of the inclusion population. A large V3 inclusion (e.g., 10,000 μm^3, corresponding to an effective diameter of approximately 27 μm) is statistically much more likely to reside close to a cut surface than a small V1 inclusion (e.g., 200 μm^3, with an effective diameter of approximately 7 μm). As the physical distance between the inclusion wall and the free surface of the thick section decreases, the confining pressure exerted by the surrounding host calcite lattice is drastically reduced. This loss of bulk structural support promotes mechanical yielding, micro-cleavage opening, and volume expansion of the inclusion under external cutting stress.

4.4 Statistical evolution of T_h distributions

Because the rates of lattice relaxation, micro-cleavage sliding, and dislocation movement are fundamentally dependent on inclusion volume, an initially symmetric, pristine population will segregate into predictable, skewed distributions under mechanical stress. We distinguish two primary scenarios:

- **Scenario 1: Size-dependent stretching.** This scenario represents preparation-induced volume expansion caused by localized mechanical vibrations and friction from a diamond saw, or down-force during initial grinding. Small V1 fluid inclusions maintain high structural resilience due to their low internal fluid mass and high surface-area-to-volume ratio, leaving them largely unaffected. In contrast, larger V2 and V3 inclusions possess expansive micro-cavity walls that experience severe localized mechanical stress from the saw blade or abrasive grit. Rather than fracturing completely, these fragile calcite walls undergo micro-plastic deformation or minor cleavage gliding, permanently expanding the cavity volume. This irreversible expansion lowers the internal fluid density, causing the subsequently measured T_h values to tail upward in direct proportion to inclusion size (Figs. 1B, 2B).
- **Scenario 2: Widespread partial leakage.** This scenario models the catastrophic yielding of the thick section and widespread micro-fracturing caused by aggressive cutting or uneven pressure application during the final polishing

https://doi.org/10.5194/egusphere-2026-6315
Preprint. Discussion started: 4 November 2026
© Author(s) 2026. CC BY 4.0 License.

stages. If a thick section is subjected to excessive physical force, the mechanical threshold of the mineral fabric is breached instantly. Inclusions positioned along active cleavage planes or near twin lamellae fail completely. Because large V3 inclusions have a much higher probability of intersecting these structural defects, they suffer widespread, chaotic partial leakage. The resulting T_h distribution exhibits a secondary, highly scattered population of elevated temperatures that completely obliterates the original environmental signal (Figs. 1C, 2C).

The comparative statistics for these specific modeling scenarios are summarized in Table 1.

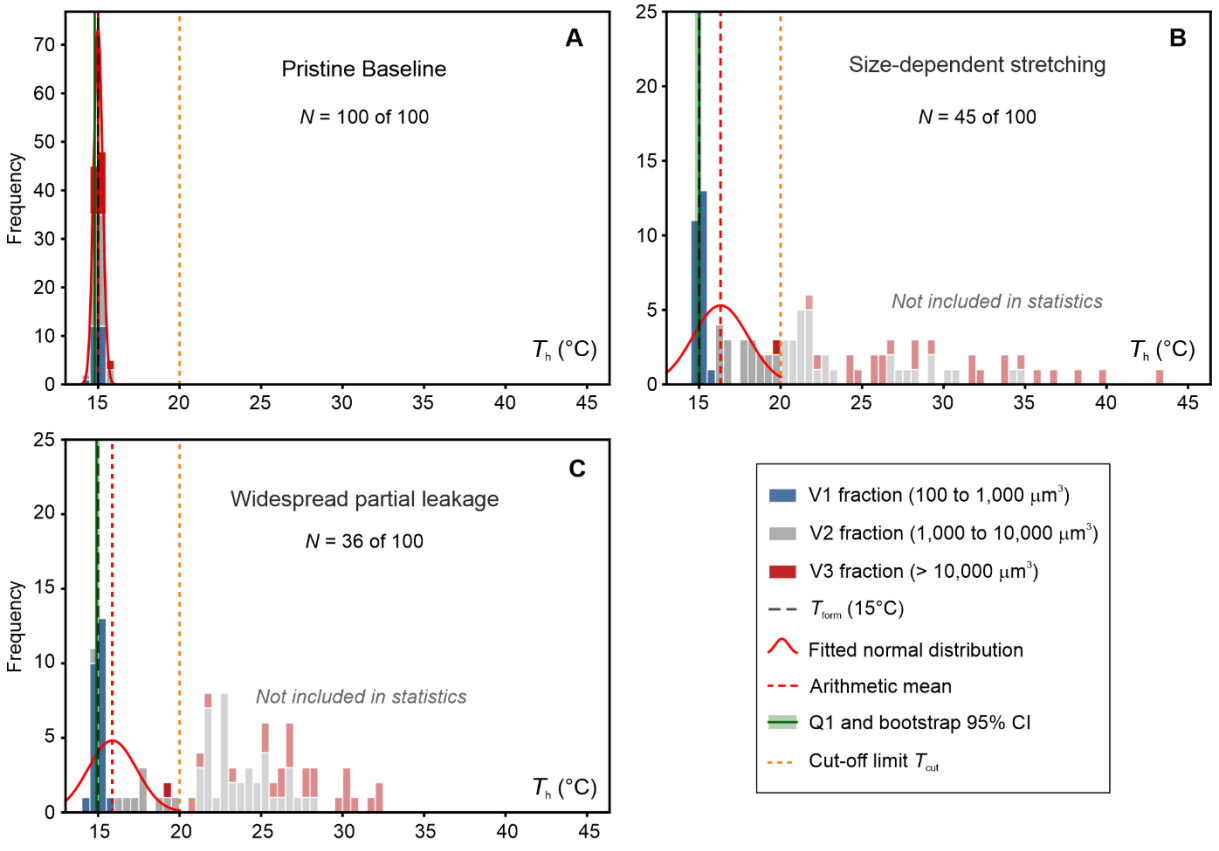


Figure 1: Synthetic stacked histograms illustrating the modification of T_h distributions under mechanical alteration. (A) Pristine baseline distribution (T_{form} = 15°C). (B) Size-dependent stretching, where the resilient V1 fraction remains anchored at T_{form} while the V2 and V3 fractions experience proportional volume stretching. (C) Widespread partial leakage resulting from high-intensity mechanical stress. Red lines indicate fitted normal distributions and their respective arithmetic means. The green line and semi-transparent band represent the first quartile (Q1) and its associated bootstrap 95% confidence interval, respectively. The vertical dashed orange line denotes an operator-defined upper cut-off limit; values exceeding this threshold are excluded from statistical calculations. Distribution statistics are compiled in Table 1.

https://doi.org/10.5194/egusphere-2026-6315
Preprint. Discussion started: 4 November 2026
© Author(s) 2026. CC BY 4.0 License.

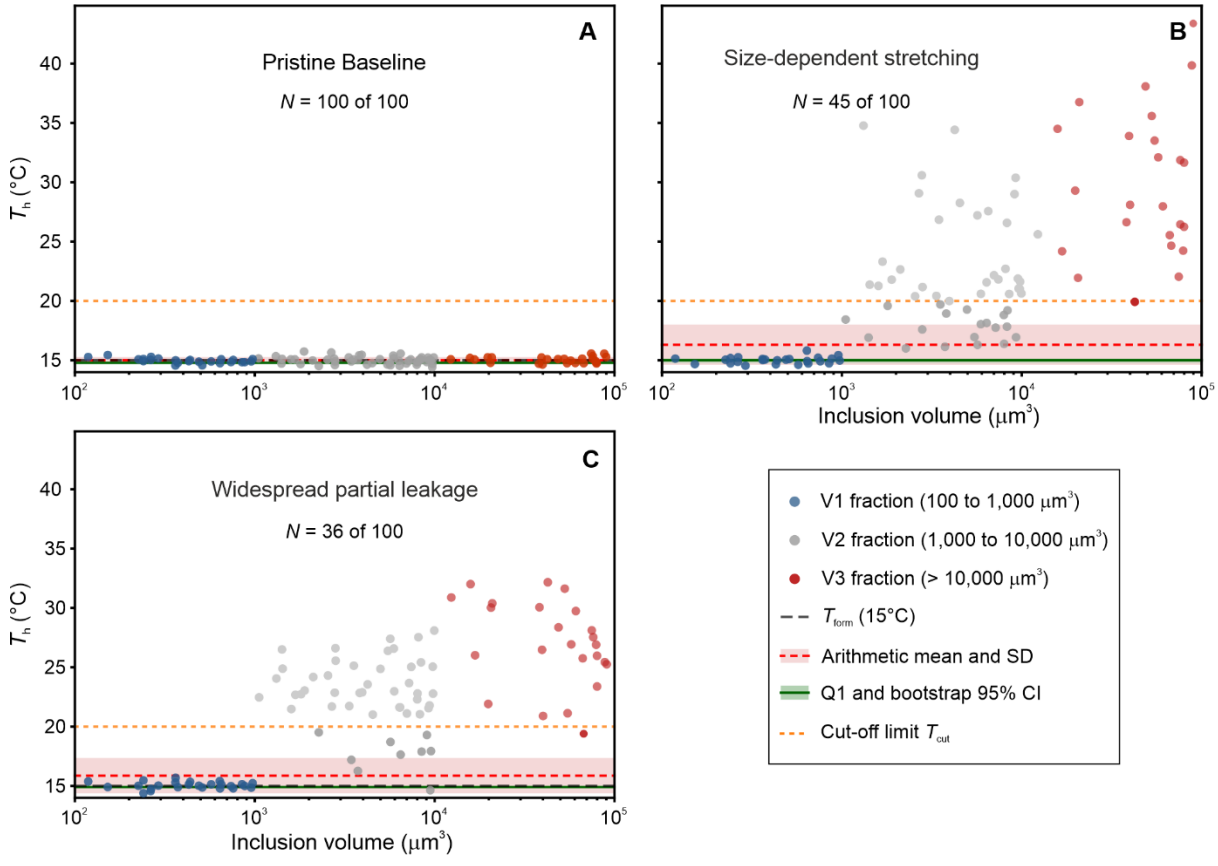


Figure 2: Synthetic inclusion volume versus T_h cross-plots illustrating mechanical alteration scenarios (initial $N = 100$ inclusions per panel). (A) Pristine baseline distribution centered at T_{form} = 15°C. (B) Size-dependent stretching, demonstrating high structural resilience in low-volume V1 inclusions and proportional stretching in the larger V2 and V3 fractions. (C) Widespread partial leakage, showing unconstrained data scattering across the larger volume fractions. Distribution statistics are compiled in Table 1.

https://doi.org/10.5194/egusphere-2026-6315
Preprint. Discussion started: 4 November 2026
© Author(s) 2026. CC BY 4.0 License.

Table 1. Statistics of distributions for mechanical, thermal, and laser-induced alteration scenarios shown in Figs. 1, 2, 4, 5, 7, and 8.

Scenario	True *T*	Mean *T*	SD	SE	Q1	IQR	95% CI Lower	95% CI Upper	$\Delta_{Mean-True_T}$	$\Delta_{Q1-True_T}$	N_r
Base case: Unaltered	15.00	15.00	0.27	0.03	14.79	0.36	14.75	14.89	0.00	–0.21	100
Mechanical: Size-dependent stretching	15.00	16.31	1.69	0.25	15.00	2.75	14.75	15.14	1.31	0.00	45
Mechanical: Widespread partial leakage	15.00	15.78	1.49	0.25	14.91	1.43	14.80	11.10	0.87	–0.09	36
Thermal: Right-skewed tail	15.00	16.70	1.63	0.19	15.11	3.17	14.98	15.44	1.70	0.11	77
Thermal: Broadened plateau	15.00	17.34	1.57	0.19	15.95	2.63	15.45	16.41	2.34	0.95	68
Laser-induced: Inverse size-dependent stretching	15.00	16.95	1.81	0.19	15.26	3.31	14.96	15.63	1.95	0.26	91
Laser-induced: Attenuated laser pulse	15.00	15.87	1.04	0.10	14.98	1.80	14.84	15.26	0.87	–0.02	100

Note. All values except *N* are in °C. The modeled scenarios assume a researcher-imposed cutoff temperature of 20°C. N_r represents the number of sample values retained after applying this cutoff, and only these retained values are used to calculate statistics.

4.5 Implications and mitigation

Investigators can systematically minimize the risk of incorporating data from cryptically stretched fluid inclusions by focusing data acquisition primarily on the smallest available fluid inclusions (V1). For larger fluid inclusions (V2 and V3), a robust diagnostic for identifying preparation-induced stretching is the rigorous evaluation of T_h values across a size gradient. A systematic increase in T_h correlated with increasing inclusion volume within a single, synchronous growth lamina serves as a clear indicator of preparation-induced stretching and should trigger the immediate rejection of the larger size fractions.

An additional diagnostic approach is spatial mapping. An increased proportion of elevated T_h values localized within inclusions situated near the cut surfaces of the sample section points directly to mechanical degradation.

5 Alteration due to exposure to elevated temperature

As NA-FIM gains broader recognition, speleothem samples formed in relatively low-temperature environments, (often near the method's lower operational limit of approximately 9°C; Krüger et al., 2011) are increasingly being analyzed. If a sample formed at T_{form} = 15°C, for example, is exposed to elevated temperatures (e.g., T_{exp} = 25°C) during transport, storage, or laboratory preparation, the resulting internal overpressure can trigger irreversible stretching of the inclusion walls. This phenomenon was demonstrated by the benchmark experiments of Krüger et al. (2011).

https://doi.org/10.5194/egusphere-2026-6315
Preprint. Discussion started: 4 November 2026
© Author(s) 2026. CC BY 4.0 License.

5.1 Thermodynamic driver of overpressure

The mechanical stability of a fluid inclusion is governed by the thermal expansion mismatch between the trapped aqueous phase and the host calcite lattice. When $T_{exp} > T_{cave}$, the fluid expands significantly more than the surrounding mineral. Within an isochoric (constant volume) system, this differential thermal expansion is converted into internal pressure (P_i). The pressure increase (ΔP) can be approximated by the thermodynamic relationship:

$$\Delta P \approx \frac{\alpha_w - \alpha_c}{\beta_w} \cdot \Delta T \quad \text{(Eq. 2)}$$

where α_w and α_c are the thermal expansion coefficients of water and calcite, respectively; β_w is the isothermal compressibility of water; and ΔT is the magnitude of temperature excursion ($T_{exp} - T_{cave}$). As illustrated in Fig. 3, thermal overpressures in fluid inclusions from low-temperature caves can exceed tens of bars. Though seemingly modest, these internal pressures frequently induce inelastic deformation in the calcite host.

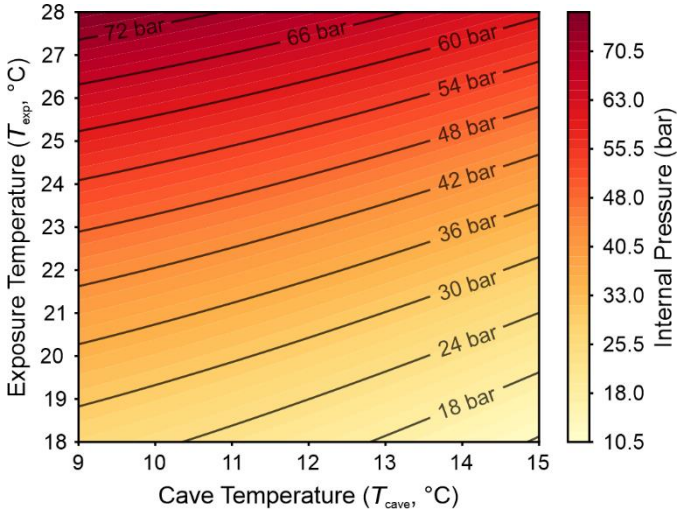


Figure 3. Thermodynamic model of internal pressure within single-phase liquid aqueous fluid inclusions in calcite, accounting for both the volumetric thermal expansion ($\alpha_{calcite}$) and elastic deformation of the host cavity. Isolines and color gradients track overpressure, calculated assuming an entrapment pressure of 1 bar.

5.2 Size-dependent susceptibility

Within the volume range typical for speleothem fluid inclusions, susceptibility to thermal stretching is non-uniform across the population. Classical elasticity suggests that hoop stress (σ_θ) at the cavity wall is independent of the absolute radius (r), as expressed by the relationship:

$$\sigma_\theta = \frac{P_i}{2} \quad \text{(Eq. 3)}$$

However, experimental evidence indicates a clear size-dependent bias. In this operational regime, large V3 inclusions (10,000 to 100,000 μm^3) are significantly more prone to "resetting" their T_h values than their smaller V1 counterparts (<1,000 μm^3) due to two primary physical reasons:

https://doi.org/10.5194/egusphere-2026-6315
Preprint. Discussion started: 4 November 2026
© Author(s) 2026. CC BY 4.0 License.

- **Statistical flaw distribution (Weibull distribution):** The probability of an inclusion wall intersecting a structural lattice defect (such as a pre-existing dislocation or a cleavage plane) scales directly with the surface area of the inclusion cavity (Weibull, 1939; Murthy et al., 2004). Larger V3 inclusions possess a much greater surface area, making them statistically more likely to host a "weakest link" where plastic yielding or micro-cracking initiates under stress.
- **Energy release rate:** According to the Griffith criterion (Griffith, 1921; Anderson, 2017), the total elastic strain energy stored within the surrounding crystal lattice is proportional to the total inclusion volume. Consequently, larger V2 and V3 inclusions provide a much larger internal energy reservoir to drive the propagation of micro-cracks or the movement of dislocations, lowering the effective pressure threshold required for irreversible volume expansion.

5.3 The role of exposure time

The total impact of elevated temperature is a joint function of the absolute magnitude of ΔT and the total duration of the thermal exposure. When samples are stored at elevated ambient conditions (such as 25°C) for extended periods lasting weeks or months, the dominant deformation mechanism shifts from an instantaneous elastic-plastic response to time-dependent re-equilibration via lattice creep.

Calcite exhibits significant dislocation creep and diffusion-assisted relaxation when subjected to sustained internal stress. Over time, the internal overpressure drives a slow, continuous increase in inclusion volume until P_i eventually relaxes toward equilibrium with the external atmospheric pressure. This long-term thermal exposure effect leads to a systematic upward drift in T_h values across the dataset, potentially masking or even erasing the original low-temperature environmental signal.

5.4 Statistical evolution of T_h distributions under thermal alteration

Because the rates of lattice relaxation, micro-cleavage sliding, and dislocation movement are fundamentally dependent on inclusion volume, an initially symmetric, pristine population will segregate into predictable, skewed distributions under thermal stress. We distinguish two primary scenarios:

- **Scenario 1: Right-skewed tail.** For samples possessing a relatively low-defect mineral fabric and featuring a continuous distribution of inclusion volumes, incomplete equilibration to thermal exposure generates a prominent positive skew. The most resilient, small-volume V1 fraction remains anchored at the baseline formation temperature, while progressively larger V2 and V3 inclusions experience proportional degrees of stretching (Figs. 4B, 5B). Importantly, while thermally induced alteration shifts T_h distributions in a manner structurally similar to mechanical size-dependent stretching, it remains fundamentally distinguished by its "capped" nature. Because thermal stretching is driven strictly by a temperature excursion (ΔT), the resulting positive tail is physically bounded by the maximum exposure temperature (T_{exp}), whereas mechanical alteration from cutting or over-polishing remains entirely "uncapped" and chaotic.

https://doi.org/10.5194/egusphere-2026-6315
Preprint. Discussion started: 4 November 2026
© Author(s) 2026. CC BY 4.0 License.

- **Scenario 2: Broadened plateau.** In poorly crystalline or highly defective calcite fabrics, high background dislocation densities dramatically lower the mechanical yielding threshold across all size fractions simultaneously. Rather than segregating cleanly by size, the entire population (encompassing V1, V2, and V3 fractions) undergoes varying degrees of volume relaxation. This widespread yielding flattens the initial Gaussian curve into a broad, high-dispersion statistical plateau with no clear modal peak (Figs. 4C, 5C).

The comparative statistics for these specific modeling scenarios are summarized in Table 1.

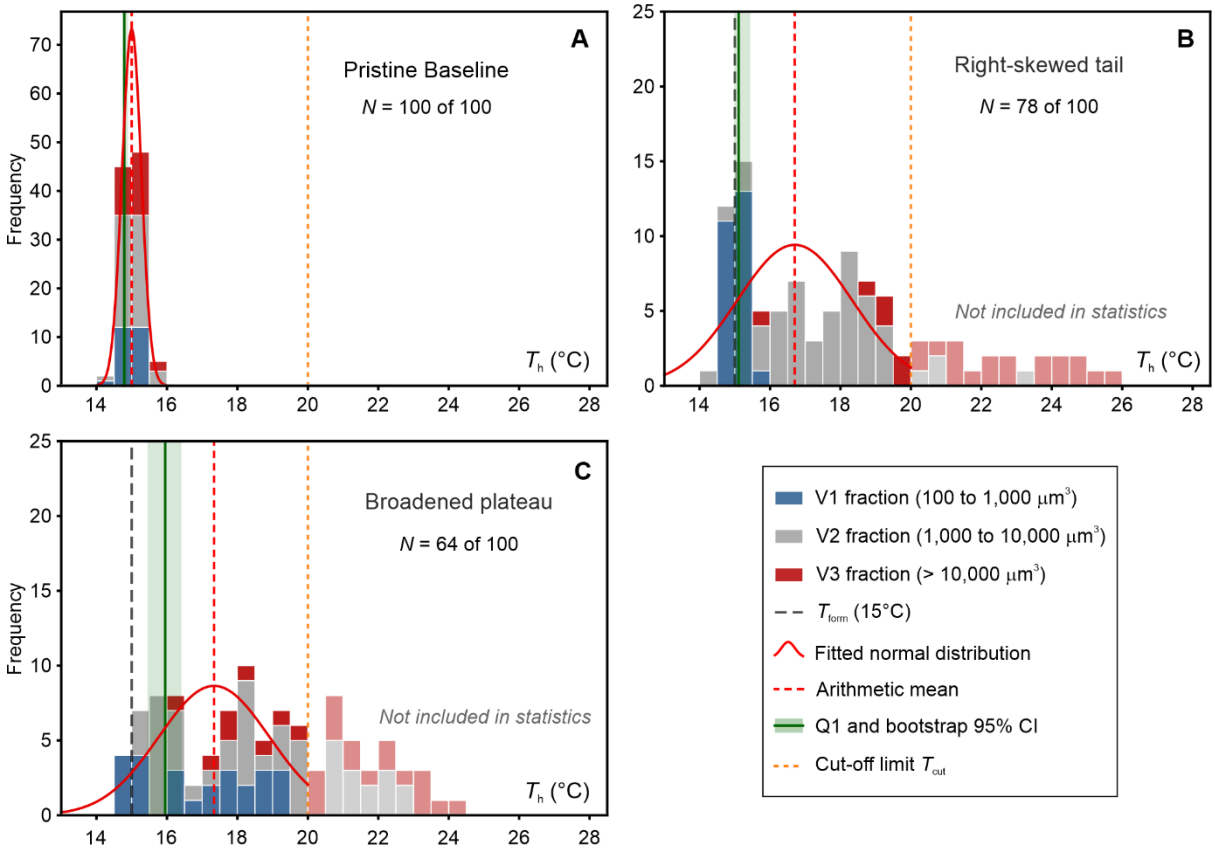


Figure 4: Synthetic stacked histograms illustrating the modification of T_h distributions under thermal alteration. (A) Pristine baseline distribution (T_{form} = 15°C). (B) Right-skewed tail resulting from partial thermal re-equilibration (T_{exp} = 25°C), where the resilient V1 fraction remains anchored at T_{form} while the V2 and V3 fractions experience proportional volume stretching. (C) Broadened plateau caused by thermal exposure within highly defective or poorly crystalline calcite fabrics, resulting in widespread volume relaxation across all size fractions. Refer to Figure 1 for descriptions of the statistical markers and the cut-off limit. Distribution statistics are compiled in Table 1.

https://doi.org/10.5194/egusphere-2026-6315
Preprint. Discussion started: 4 November 2026
© Author(s) 2026. CC BY 4.0 License.

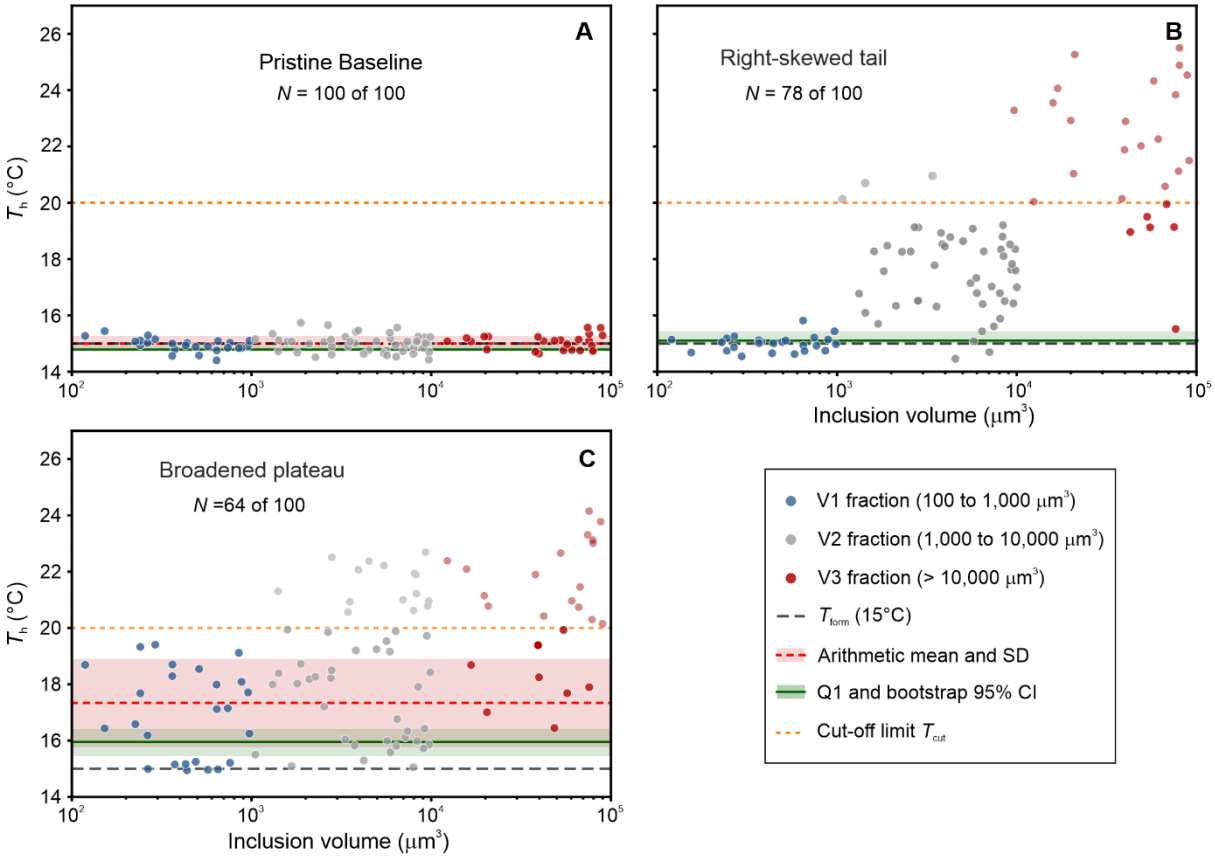


Figure 5: Synthetic inclusion volume versus T_h cross-plots illustrating thermal alteration scenarios (initial N = 100 inclusions per panel). (A) Pristine baseline distribution centered at T_{form} = 15°C. (B) Right-skewed tail during partial thermal re-equilibration (T_{exp} = 25°C), demonstrating high structural resilience in V1 inclusions and a positive, size-dependent stretching trend in the larger V2 and V3 fractions. (C) Broadened plateau in highly defective fabrics, showing widespread, unconstrained volume relaxation across all size fractions. Distribution statistics are compiled in Table 1.

5.5 Implications and mitigation

Potential post-entrapment exposure to elevated temperatures is particularly critical for speleothem records from cold mid-latitude or alpine caves, where the temperature differential (ΔT) between the true T_{form} and subsequent exposure (T_{exp}, such as temperature during transport or storage) is largest. In contrast, this specific mechanism is less relevant for tropical speleothem samples where the original formation temperature closely matches typical room temperature ($T_{form} \approx T_{exp}$).

To prevent post-entrapment alteration, we strongly recommend that speleothem samples be transported and stored at controlled temperatures below their true formation temperature ($T < T_{form}$) immediately following field collection. This practice keeps the fluid inclusions in a state of relative underpressure, preventing the thermodynamic initiation of wall stretching.

While continuous refrigeration is the ideal preventive measure, it is often logistically impossible due to the practical realities of fieldwork, shipping, and long-term archiving. Importantly, a failure to maintain strict temperature control does not render

https://doi.org/10.5194/egusphere-2026-6315
Preprint. Discussion started: 4 November 2026
© Author(s) 2026. CC BY 4.0 License.

samples from low-temperature caves unsuitable for analysis. Even if a sample has been compromised by thermal exposure, researchers can still extract robust paleotemperature data by employing the following analytical protocols:

- **Identify potential thermal alteration** within the dataset by rigorously analyzing the statistical skewness and the size-dependence of the acquired T_h dataset across a V1-to-V3 volume gradient.
- **Filter the raw dataset** to isolate the pristine signal, utilizing the smallest available inclusion fractions (the V1 size class) as the most texturally and structurally reliable.

6 Laser-induced alteration

A characteristic data pattern in inclusion volume versus T_h space (defined by a distinct negative correlation slope) was first reported by Spadin et al. (2015) and has since been repeatedly observed by many researchers, including the present author. In sharp contrast to alteration driven by post-entrapment mechanical impact or thermal exposure, where the smallest fluid inclusions demonstrate the highest resilience, these specific distributions exhibit an inverted trend: the smallest inclusions consistently yield the highest T_h values. Crucially, in the benchmark case study by Spadin et al. (2015), where the true formation temperature was independently constrained, the smallest inclusions would have been thermodynamically incapable of nucleating vapor bubbles had they remained truly unaltered. We interpret this anomalous, size-dependent vulnerability as mechanical stretching induced directly by the analytical laser pulses during excitation.

6.1 Spatial energy distribution and shockwave propagation

A femtosecond laser pulse deposits a discrete, highly localized packet of optical energy into the confined aqueous volume of the inclusion. A fraction of this incident energy is converted into transient mechanical energy through rapid plasma formation, explosive thermoelastic expansion, and the subsequent generation of an acoustic shockwave (Vogel et al., 2005; Linz et al., 2025).

The physical impact of this shockwave on the surrounding inclusion walls is strictly governed by the distance it travels from the laser's focal point. In larger V3 inclusions, the shockwave travels farther through the aqueous medium, experiencing significant geometric attenuation and viscous damping before reaching the host crystal interface. Experimental studies of laser-generated shockwaves in water demonstrate that peak pressure decays approximately as $1/r$ at distances beyond 150 µm from the source (Noack and Vogel, 1995; Chemin et al., 2022), which is consistent with classical acoustic attenuation models in liquids. In contrast, in small V1 inclusions, the focal point is positioned in extreme proximity to the cavity walls. The shockwave consequently arrives at the mineral interface with near-peak pressure, subjecting the local crystal lattice to an intense, high-velocity mechanical stressor.

https://doi.org/10.5194/egusphere-2026-6315
Preprint. Discussion started: 4 November 2026
© Author(s) 2026. CC BY 4.0 License.

6.2 Specific mechanical stress and inclusion integrity

The total energy of the laser pulse in an NA-FIM setup is fine-tuned using a rotatable half-wave plate combined with a fixed Glan-laser polarizer (Arnuk et al., 2024). Specific mechanical stress (S_m) represents the volumetric energy density (the total amount of optical energy trapped within the micro-cavity), which serves as the primary driver for potential host mineral deformation during bubble nucleation. This relationship can be expressed conceptually as:

$$S_m = \frac{E_{source} \cdot R_{split} \cdot sin^2(\theta)}{V_{inclusion}} \quad \text{(Eq. 4)}$$

where E_{source} is the base pulse energy (determined by a 20 mW laser power setting); R_{split} represents the 10:90 beam splitter ratio; $sin^2\theta$ represents the non-linear transmission governed by the polarizer angle theta; and $V_{inclusion}$ is the cavity volume. The energy densities generated by a single NA-FIM laser pulse across different inclusion volumes are illustrated in Fig. 6.

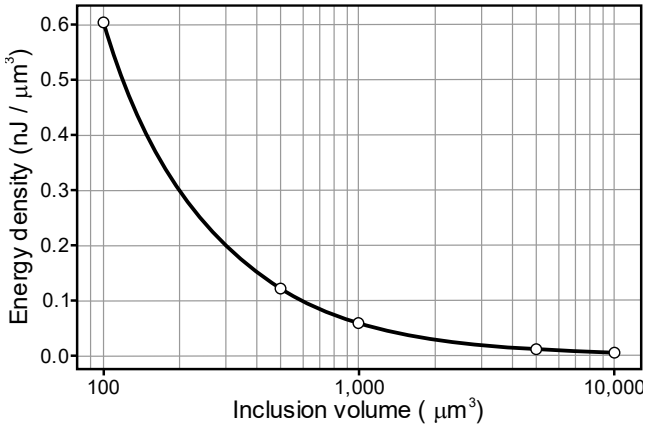


Figure 6: Calculated mechanical energy density delivered into fluid inclusion cavities of varying volumes by a single 200-femtosecond laser pulse. The calculation is based on a baseline laser source power of 20 mW, a source pulse energy of 20,000 nJ, a 10:90 beam split ratio, and a 10° polarizer opening angle. The plot highlights the severe, non-linear concentration of shockwave energy within the smallest inclusion volumes (the V1 size class).

In small V1 inclusions, the resulting pressure spike can easily exceed the elastic limit or the yield strength of the host calcite. Because calcite possesses perfect cleavage and low hardness, it is highly prone to plastic deformation or microscopic displacement along twinning planes under these high localized energy densities. Even a negligible, sub-micron increase in the cavity's volume drastically lowers the fluid density, shifting the subsequently measured T_h toward artificially higher values.

6.3 The influence of inclusion morphology on mechanical failure

In addition to absolute inclusion volume, the specific morphology of the cavity serves as a critical determinant of mechanical stability during NA-FIM laser impacts. Our observations indicate that the risk of laser-induced stretching, even within relatively large V2 and V3 inclusions, is significantly exacerbated in inclusions with erratic, non-equilibrated forms.

https://doi.org/10.5194/egusphere-2026-6315
Preprint. Discussion started: 4 November 2026
© Author(s) 2026. CC BY 4.0 License.

While nearly isometric, spherical, or negative-crystal vacuoles distribute internal pressure spikes evenly across their boundary surfaces, inclusions possessing sharp corners, elongated necks, or wedge-shaped reentrants act as potent stress concentrators. According to the principles of linear elastic fracture mechanics, mechanical stress intensifies dramatically at points of high boundary curvature. In these irregular inclusions, even a relatively attenuated shockwave (such as those propagating through larger internal volumes) can generate localized stresses at sharp reentrants that breach the tensile strength of the host mineral, leading to irreversible volumetric expansion.

6.4 Statistical evolution of T_h distributions under laser-induced alteration

Our modeling of the statistical evolution of T_h distributions under laser-induced stress is based on three core physical premises:

- **Inverse shock susceptibility:** Laser shockwave energy density concentrates most intensely within the smallest cavity volumes. Peak stress intensity at the inclusion-host interface is inversely proportional to cavity volume, meaning V1 inclusions suffer the most severe physical disruption.
- **Chaotic failure:** Laser shock stress alters inclusion volume by rapidly "unzipping" cleavage planes or mobilizing dislocations. The resulting upward shifts in T_h are therefore open-ended and variable.
- **Large inclusions as attenuation sinks:** Large V3 cavities possess sufficient internal fluid path length to attenuate the laser shockwave before critical failure stresses develop at the water-calcite interface, preserving the original environmental formation signal.

We distinguish two primary modeling scenarios.

- **Scenario 1: Inverse size-dependent stretching.** This scenario represents a case where the femtosecond laser's pulse energy is set too high for small inclusion geometries, causing an accidental volume increase during the bubble nucleation attempt. In contrast, large V2 and V3 inclusions possess a sufficient volume buffer that dampens the localized mechanical shockwave safely, ensuring that bubble nucleation occurs without altering the inclusion volume (Figs. 7B, 8B).
- **Scenario 2: Attenuated laser pulse.** This scenario models a perfectly optimized, low-fluence femtosecond laser workflow. A sufficiently attenuated laser pulse delivers exactly enough mechanical energy to induce acoustic cavitation and nucleate the shrinkage bubble but stops safely short of the calcite host's structural yield threshold. The minimal mechanical overprint is restricted to the highest-curvature margins of the smallest V1 inclusions, which register only negligible volume changes. The larger V2 and V3 size classes undergo bubble nucleation with no geometric deformation (Figs. 7C, 8C).

The comparative statistics for these laser alteration scenarios are summarized in Table 1.

https://doi.org/10.5194/egusphere-2026-6315
Preprint. Discussion started: 4 November 2026
© Author(s) 2026. CC BY 4.0 License.

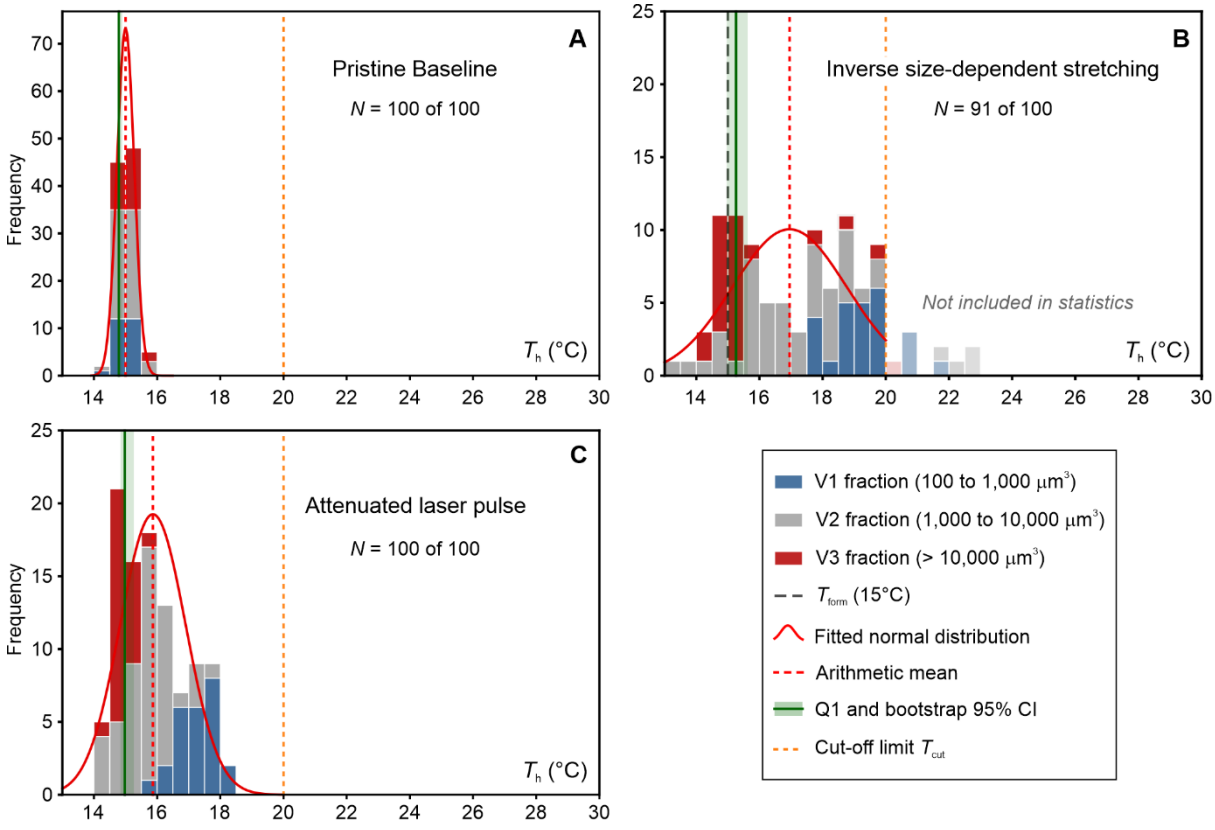


Figure 7: Synthetic stacked histograms illustrating the modification of T_h distributions under laser-induced alteration. (A) Pristine baseline distribution (T_{form} = 15°C). (B) Inverse size-dependent stretching caused by excessive pulse energy, where the vulnerable V1 fraction is maximally affected by physical disruption while the larger V3 fractions safely buffer the acoustic shockwave. (C) Attenuated laser pulse representing a well-tuned intensity, where minimal mechanical overprint is restricted to the highest-curvature margins of the smallest V1 inclusions while larger size classes undergo bubble nucleation with zero geometric deformation. Refer to Figure 1 for descriptions of the statistical markers and the cut-off limit. Distribution statistics are compiled in Table 1.

https://doi.org/10.5194/egusphere-2026-6315
Preprint. Discussion started: 4 November 2026
© Author(s) 2026. CC BY 4.0 License.

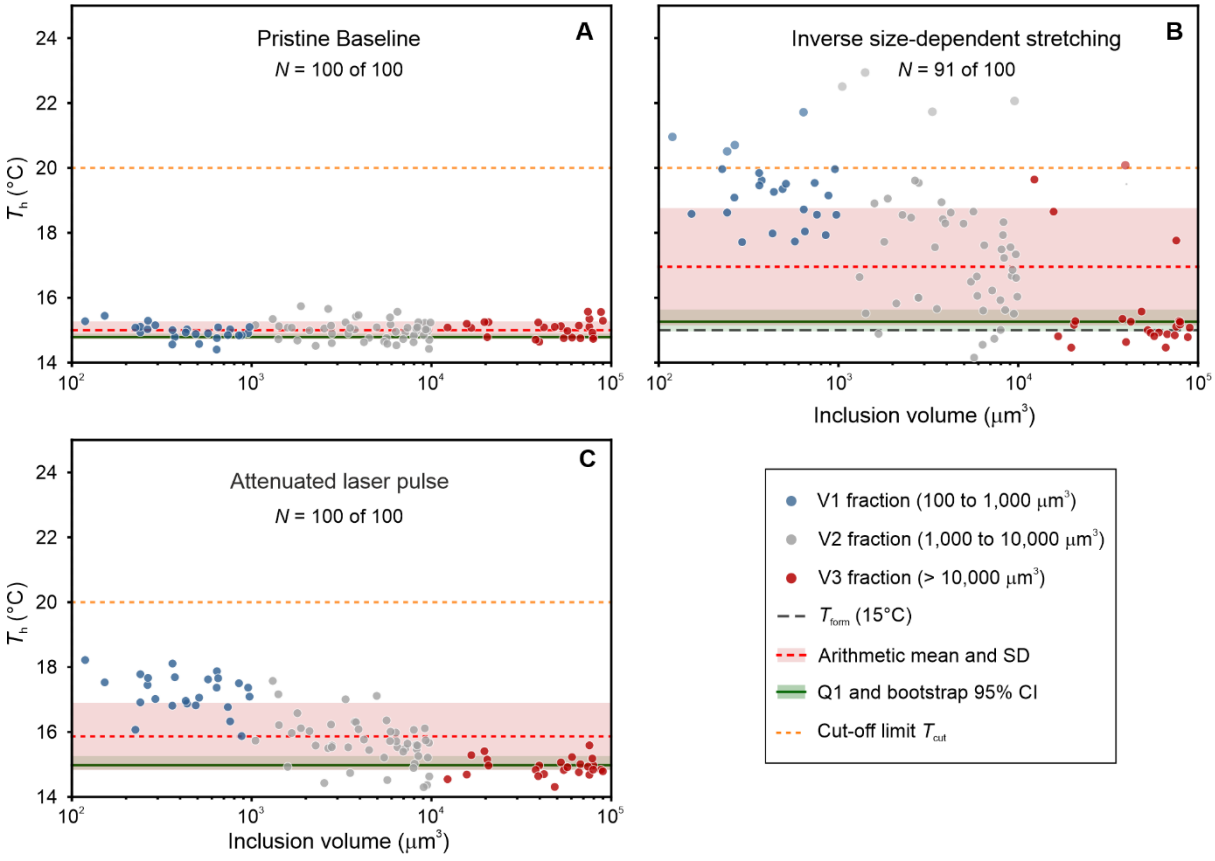


Figure 8: Synthetic inclusion volume versus T_h cross-plots illustrating laser-induced alteration scenarios (initial N = 100 inclusions per panel). (A) Pristine baseline distribution centered at T_{form} = 15°C. (B) Inverse size-dependent stretching under excessive pulse energy, demonstrating severe mechanical disruption and positive T_h shifting within low-volume V1 inclusions while larger V3 fractions safely buffer the acoustic shockwave. (C) Attenuated laser pulse using a well-tuned intensity, demonstrating an optimized protocol where minimal mechanical overprint is restricted to the smallest V1 size class while larger fractions undergo bubble nucleation with zero geometric deformation. Distribution statistics are compiled in Table 1.

6.5 Implications and mitigation

For paleoclimate investigators employing NA-FIM protocols, recognizing laser-induced stretching is essential to avoid artificial warm biases that selectively corrupt the smallest inclusion records.

- **Analytical awareness:** Additional screening care must be taken when analyzing fluid inclusions in the smallest size class (V1, <1,000 µm³). Because of their heightened vulnerability to laser shock, evaluating T_h values along a V1-to-V3 volume gradient serves as a critical diagnostic check.
- **Laser energy optimization**: While operating at the lowest laser power sufficient for bubble nucleation (typically controlled via narrow opening angles on the Glan-laser polarizer) is always standard practice, this low-fluence approach is especially vital when targeting small cavities.

https://doi.org/10.5194/egusphere-2026-6315
Preprint. Discussion started: 4 November 2026
© Author(s) 2026. CC BY 4.0 License.

Unlike thermal or mechanical stress fields, which spare small inclusions while preferentially altering large V3 cavities, analytical laser pulses selectively target the smallest V1 inclusions. Identifying a negative T_h-versus-volume slope is therefore essential for isolating true formation conditions and ensuring that laser-induced overprints are not mistaken for primary paleoclimate signals. Crucially, this laser-specific resilience does not imply universal stability. While large V3 inclusions routinely escape analytical laser damage, they are precisely the most vulnerable to stretching under thermal and mechanical stress fields (Section 7).

7 The combined effect of multiple stressors

While the mechanical, thermal, and laser-induced alteration mechanisms have been evaluated independently in the preceding sections, they operate sequentially (and often synergistically) within practical NA-FIM studies. In natural speleothems, the structural degradation of a fluid inclusion assemblage does not occur in isolation; rather, each subsequent stressor exploits and amplifies the structural damage initiated by its predecessor.

This synergistic coupling is most pronounced in speleothems formed in low-temperature mid-latitude or alpine caves ($T_{form} \approx$ 9–15°C). When such a sample is extracted and brought to a standard laboratory environment ($T_{exp} \approx$ 25°C), the thermal expansion mismatch between the fluid inclusion water and the host calcite immediately generates a static, isotropic internal overpressure of approximately 40–55 bar (Krüger et al., 2011; Fig. 3). At this stage, before any sample preparation or analytical measurements have begun, the cavity walls of the entire inclusion population are already under significant tensile stress, acting as a pre-loaded thermodynamic spring.

When the sample undergoes physical preparation (low-speed sawing and grinding), the external mechanical shear stress (σ_{mech}) is focused onto these pre-pressurized inclusion walls. According to continuum mechanics, the effective yield threshold ($\sigma_{y,eff}$) of the host calcite is reduced in direct proportion to the pre-existing internal overpressure (P_i) and the geometric stress concentration factor (K_t; cf. Eq. 1):

$$\sigma_{y,eff} = \sigma_y - (K_t \cdot P_i) \quad \text{(Eq. 5)}$$

Because irregular morphology or sharp reentrants can elevate K_t significantly (K_t values of 3 or higher), a nominal 40–55 bar thermal overpressure is geometrically amplified at cavity corners, lowering the additional external force required for mechanical failure by well over 100 bar. Consequently, irreversible volume stretching occurs under minor mechanical loads that a pristine, non-overpressured sample would easily tolerate without deformation.

The climax of this synergistic cascade occurs during NA-FIM analysis. When an ultra-short femtosecond laser pulse is focused into a small, pre-pressurized V1 inclusion to force bubble cavitation, the transient, high-velocity dynamic shockwave pressure (ΔP_{laser}) superimposes directly onto a system already operating near its physical breaking point. The combined stress tensor instantly breaches the yield threshold of the calcite host:

$$K_t \cdot (P_i + \sigma_{mech}) + \Delta P_{laser} > \sigma_y \quad \text{(Eq. 6)}$$

https://doi.org/10.5194/egusphere-2026-6315
Preprint. Discussion started: 4 November 2026
© Author(s) 2026. CC BY 4.0 License.

This multi-stage overprinting creates a severe multiplier effect: the thermal overpressure primes the lattice, mechanical handling introduces sub-critical micro-fractures, and the laser pulse triggers final structural yielding. This compound vulnerability explains why non-ideal, right-skewed distributions must be expected in low-temperature speleothems, and underscores the absolute necessity of utilizing a robust, directionally conservative statistical metric, such as the first quartile (Q1), to isolate the uncompromised paleoclimate signal.

8 Practical software implementation

In this section, we provide practical guidance on integrating the statistical approach outlined above into routine fluid inclusion protocols. Crucially, adopting this methodology requires no alterations to existing laboratory procedures; all physical steps of NA-FIM data acquisition remain exactly the same.

At the primary facility where NA-FIM analysis is presently conducted (the Fluid Inclusion Laboratory within the Department of Earth Sciences at the University of Bergen, Norway), initial data processing is performed using custom MATLAB software (Pasqualetto et al., in preparation). The output of this initial processing is an Excel file containing data on the radii of nucleated bubbles, calculated fluid inclusion volumes, and Laplace-corrected T_h values.

To seamlessly integrate our proposed statistical approach, we have developed a custom Python script that directly ingests this MATLAB output and visualizes the results for immediate inspection (Dublyansky, 2026b). The script provides the following automated analytical steps:

- **Data visualization:** The acquired T_h values are displayed as standard histograms and volume cross-plots, with the distinct inclusion size classes (V1, V2, and V3) discriminated by color to easily identify size-dependent alteration trends.
- **Normality assessment:** The software includes options for formal statistical testing of normality, alongside visual assessment via Quantile-Quantile (Q-Q) plots, which readily highlight deviations from a theoretical normal distribution (particularly at the tails).
- **Metric comparison:** Traditional parametric metrics (arithmetic mean and standard deviation) and the proposed robust estimators (Q1 and bootstrap 95% confidence intervals) are natively calculated. These metrics are superimposed directly onto the graphs, allowing for an immediate visual comparison of their performance.

Finally, the complete set of generated statistical metrics is appended directly back into the initial Excel file for archiving and subsequent use.

9 Conclusions

Fluid inclusions in speleothems are highly vulnerable to post-entrapment alteration driven by three distinct stressors: mechanical stress associated with sample preparation (sectioning, grinding, and polishing); thermal re-equilibration when low-

https://doi.org/10.5194/egusphere-2026-6315
Preprint. Discussion started: 4 November 2026
© Author(s) 2026. CC BY 4.0 License.

temperature samples are exposed to elevated ambient conditions during transport, storage, and analysis; and direct laser impact during NA-FIM data acquisition. While thermal re-equilibration plays a limited role in speleothems formed at relatively high temperatures (20–25°C), it acts as a potent structural multiplier in samples formed at lower temperatures (9–15°C), systematically enhancing their vulnerability to both mechanical preparation and laser-induced stress.

The physical consequence of these alterations is that individual inclusions either become stretched via irreversible cavity expansion or partially lose their water via micro-leakage. Both forms of structural failure cause a corresponding decrease in the density of the entrapped water, forcing altered inclusions to yield erroneously elevated homogenization temperatures (T_h). Strictly speaking, such compromised inclusions no longer represent true isochoric systems.

The response of measured T_h distributions to these three alteration mechanisms depends on the intensity of the specific stressor, the fabric of the host speleothem, and the geometric properties (volume and shape) of the inclusions themselves. Critically, all three alteration mechanisms elicit a fundamentally similar statistical response: the initially symmetrical, Gaussian T_h distributions characteristic of pristine samples distort into asymmetric profiles with varying degrees of positive skew. Consequently, traditional parametric metrics (such as the arithmetic mean, standard deviation, and standard error) become mathematically compromised and systematically overestimate the true formation temperature.

While specific types of post-entrapment alteration can be identified under idealized conditions by evaluating characteristic distribution patterns and size-dependent trends, practical limitations often interfere. At the relatively small sample sizes typical of routine fluid inclusion research (20–40 measurements per growth band), formal statistical tests lack sufficient power to reliably detect non-normality or minor positive skew. Consequently, researchers must rely on visual inspection of T_h distributions, an approach that is inherently subjective.

A conservative and consistent solution under these circumstances is the uniform application of the first quartile (Q1) as the primary estimator of the true formation temperature (T_{form}) across all samples. This strategy ensures strictly objective, uniform treatment across entire time series datasets, eliminates subjective investigator decisions regarding which specific distributions appear "sufficiently normal" to warrant metric switching, and guarantees that positive overestimations due to post-entrapment alteration are minimized. For perfectly unbiased, pristine normal distributions, using Q1 underestimates the true arithmetic mean by a stable offset of approximately 0.67 standard deviations, representing a minor, fully quantifiable, and directionally conservative trade-off that safeguards the integrity of paleoclimate reconstructions.

https://doi.org/10.5194/egusphere-2026-6315
Preprint. Discussion started: 4 November 2026
© Author(s) 2026. CC BY 4.0 License.

Appendix A Modeling of mechanical alteration

The synthetic data modeling for mechanical disturbance represents the chaotic structural alteration of fluid inclusions during sample preparation (such as precision sawing, grinding, or polishing). This methodology encodes the "kinetic failure" hypothesis, where the primary driver of T_h shifts is the stochastic interaction between external mechanical stress fields and the mineral's internal cleavage planes.

The interactive implementation of this model and its visualization parameters are available in the simulation suite (1_mechanical_alt.py; Dublyansky, 2026a).

Core concepts governing the model

The mechanical disturbance model is governed by three physical principles:

1. **Geometric probability of failure:** The model assumes that larger inclusions have a significantly higher statistical probability of intersecting a pre-existing cleavage plane, twin lamella, or stress-induced micro-fracture. This creates a size-dependent vulnerability, where larger cavities are the primary targets of post-entrapment alteration.
2. **Chaotic, kinetic failure (uncapped):** Unlike thermal stretching, mechanical disturbance is a kinetic process rather than a thermodynamic one. Consequently, it is not bounded by an external temperature ceiling. Irreversible volume stretching can be extreme and highly unpredictable, depending on the random orientation of the inclusion relative to the applied stress field.
3. **Resilience of micro-cavities:** Small inclusions are modeled as safely nested within intact, defect-free crystal blocks, making them highly resilient to preparation-induced mechanical stress.

Mathematical generation of mechanical alteration scenarios

In speleothem fluid inclusion research, mechanical alteration is artificial, produced almost exclusively during sample preparation. Because speleothem calcite is relatively soft and highly cleavable, it is vulnerable to the mechanical stresses encountered during laboratory processing (such as cutting thick blocks with a low-speed diamond saw, followed by manual grinding and polishing to create 300–400 μm-thick sections).

When these preparation procedures breach the mechanical shear thresholds of the host calcite fabric, a user-defined percentage of inclusions within each size class yields. While the pristine fraction preserves the baseline formation temperature (T_{form} = 15°C), the altered fraction experiences irreversible volume stretching or partial fluid leakage driven by micro-fracturing. This forces T_h values upward into an open-ended, positively skewed distribution.

https://doi.org/10.5194/egusphere-2026-6315
Preprint. Discussion started: 4 November 2026
© Author(s) 2026. CC BY 4.0 License.

Scenario 1: Open-ended right-skew (high variance)

Mathematical Formulation

- **V1 size class (< 1,000 µm³):** The altered fraction undergoes a mild, low-variance, high-temperature shift modeled via a right-clipped normal distribution (mean = 15.0°C, SD = 0.6°C).
- **V2 size class (1,000 to 10,000 µm³):** The altered fraction shifts past the baseline using a highly skewed, open-ended Gamma distribution (shape = 2.5, scale = 2.5), anchored at T_{form}.
- **V3 size class (10,000 to 100,000 µm³):** The altered fraction shifts even further using an aggressive, high-spread Gamma distribution (shape = 5.0, scale = 2.8).
- **Boundary Constraints:** No upper truncation limit is applied. The synthetic data naturally tapers off past 30°C, successfully reflecting an asymmetric, positively skewed continuum.

Physical Interpretation

During section slicing, mechanical kinetic energy transfers directly into the calcite lattice. Small V1 fluid inclusions maintain high structural resilience due to their low total internal fluid mass and high surface-area-to-volume ratio, leaving them mostly unaffected. In contrast, larger V2 and V3 inclusions possess wide micro-cavity walls that experience severe localized mechanical stress from applied loads (such as the saw blade or abrasive grit). Rather than fracturing completely, these fragile calcite walls undergo micro-plastic deformation or minor cleavage gliding, irreversibly expanding the cavity volume. This irreversible volume expansion drops the internal fluid density, forcing the subsequently measured homogenization temperatures (T_h) to tail upward past the true environmental formation baseline (T_{form}) in direct proportion to inclusion size.

Scenario 2: Dispersed bimodal failure (unbounded clusters)

Mathematical Formulation

Rather than tracking a smooth mathematical continuum, this scenario models a distinct, high-variance disruption using independent, open-ended normal distributions across the size classes:

- **V1 size class (< 1,000 µm³):** The population remains entirely resistant, retaining a tight, pristine normal distribution centered at the baseline (T_{form} = 15°C).
- **V2 size class (1,000 to 10,000 µm³):** The altered fraction shifts entirely into an elevated, high-variance normal distribution centered at a mean = 22.0°C with a broad spread (SD = 3.0°C).
- **V3 size class (10,000 to 100,000 µm³):** The altered fraction breaks away completely into a major high-temperature cluster centered at a mean = 27.0°C with an even wider dispersion (SD = 3.5°C).

https://doi.org/10.5194/egusphere-2026-6315
Preprint. Discussion started: 4 November 2026
© Author(s) 2026. CC BY 4.0 License.

Physical Interpretation

This scenario models catastrophic thick section yielding and micro-fracturing due to aggressive cutting or uneven pressure applied during the final polishing stages. Calcite possesses perfect cleavage, making speleothem sections highly prone to micro-faulting when subjected to lateral grinding forces. If a thick section catches slightly on a polishing lap or is subjected to excessive manual down-force, the mechanical yield threshold of the mineral fabric is breached instantly.

Inclusions positioned along active cleavage planes or near twin lamellae fail completely. Because large V3 inclusions have a much higher statistical probability of intersecting these open crystal dislocations, they suffer widespread, chaotic partial leakage. Fluid leaks out of the inclusion cavities until the external stress is removed and the micro-fractures physically close, leaving behind a highly scattered, high-temperature bimodal cluster that completely obliterates the original 15.0°C paleotemperature signal.

Appendix B: Modeling of incomplete thermal re-equilibration

The synthetic data modeling for thermal re-equilibration was designed to represent the classic thermodynamic behavior of fluid inclusions subjected to post-depositional heating. This methodology encodes the "orderly stretching" hypothesis, where volumetric cavity expansion is a predictable function of inclusion size and internal thermodynamic overpressure. The modeling results are presented in two synchronized graphical forms: inclusion volume versus T_h cross-plots and stacked histograms illustrating the evolution of the T_h distribution.

The interactive implementation of this model and its visualization parameters are available in the simulation suite (2_thermal_alt.py; Dublyansky, 2026a).

Core concepts governing the modeling framework

The thermal re-equilibration model is governed by three physical principles:

1. **Direct size-dependent susceptibility:** The model assumes that larger fluid inclusions are more susceptible to internal overpressure. As the host mineral is heated, the internal pressure within large cavities more easily breaches the host calcite's elastic limit, leading to dislocation glide and irreversible volume expansion.
2. **Thermodynamic limit (The "ceiling" effect):** Unlike the uncapped nature of mechanical stress fields or laser shockwaves, thermal stretching is a structural relaxation process governed by a strict thermodynamic equilibrium. The maximum possible T_h shift is physically capped by the peak environmental exposure temperature (T_{exp}). Altered inclusions "reach" for this temperature but do not exceed it.
3. **Small inclusions as rigid anchors:** Small inclusions are modeled as structurally robust. High surface-energy thresholds and the intrinsic crystal strength of the surrounding calcite matrix prevent stretching at moderate internal overpressures, ensuring they preserve the primary environmental formation signal.

https://doi.org/10.5194/egusphere-2026-6315
Preprint. Discussion started: 4 November 2026
© Author(s) 2026. CC BY 4.0 License.

Mathematical generation of alteration scenarios

In this approach, all scenarios begin with an initial, unaltered baseline sample population. This baseline control is generated using a normal (Gaussian) distribution centered at the true formation temperature (T_{form} = 15.0°C) with a tight analytical standard deviation (SD = 0.3°C).

When an alteration scenario is triggered, a user-defined percentage of inclusions within each size class is dynamically partitioned. The pristine fraction remains anchored around 15.0°C, while the altered fraction is subjected to mathematical modifications that simulate stretching, leakage, or volume relaxation.

Scenario 1: Continuous size-dependent stretching

Mathematical Formulation

- **V1 size class (< 1,000 µm³):** he altered fraction experiences zero net thermodynamic shift, modeled via a clipped normal distribution centered at the baseline (15.0°C, SD = 0.3°C).
- **V2 size class (1,000 to 10,000 µm³):** The altered fraction is drawn from an elevated normal distribution (mean = 17.5°C, SD = 1.5 °C).
- **V3 size class (10,000 to 100,000 µm³):** The altered fraction is drawn from an extreme high-temperature normal distribution (mean = 22.0°C, SD = 2.0°C).
- **Boundary Constraints:** To prevent unphysical data generation beyond the thermal limits of the event, all shifted values across all size classes are strictly truncated using an array-clipping function to a maximum threshold slightly above the exposure temperature (T_{exp} + 0.5°C = 25.5°C).

Physical Interpretation

This scenario represents a progressive thermal overprinting or overheating event under moderate internal overpressure. In nature, smaller inclusions have a higher surface-area-to-volume ratio and lower total internal fluid mass, giving them greater mechanical resilience against internal overpressure. Conversely, larger inclusions experience much higher mechanical hoop stress along their walls at elevated temperatures. As the host speleothem is heated toward 25°C, the largest inclusions yield first, micro-fracturing or plastically stretching their host cavities to irreversibly increase their volumes. This irreversible volume expansion lowers the internal fluid density, artificially shifting the subsequently measured homogenization temperatures (T_h) upward toward the exposure temperature. The resulting asymmetric, positively skewed tail is directly proportional to inclusion size.

https://doi.org/10.5194/egusphere-2026-6315
Preprint. Discussion started: 4 November 2026
© Author(s) 2026. CC BY 4.0 License.

Scenario 2: Broadened plateau (high-defect fabric)

Mathematical Formulation

Rather than using traditional normal distributions to model the overprint, this scenario utilizes bounded uniform (flat) distributions combined with a baseline Gaussian noise component:

- **V1 size class (< 1,000 µm³):** The altered fraction is spread evenly between a lower limit of 14.8°C and an upper limit of 19.5°C.
- **V2 size class (1,000 to 10,000 µm³):** The altered fraction is spread evenly between a lower limit of 15.0°C and an upper limit of 22.5°C.
- **V3 size class (10,000 to 100,000 µm³):** The altered fraction is spread evenly between a lower limit of 16.5°C and an upper limit of 24.5°C.
- **Analytical Noise:** Every shifted data point is subsequently jittered by adding a random Gaussian noise factor (mean = 0, SD = 0.3°C) to simulate natural variations and measurement limitations.

Physical Interpretation

This scenario represents widespread volume relaxation and partial leakage within a highly defective, poorly crystalline speleothem fabric. In such conditions, fluid inclusions cease to behave as isolated, rigid ideal systems. Instead, fluids leak at highly variable rates along dense networks of micro-structural defects, or the inclusion walls deform unevenly based on their immediate proximity to crystal dislocations or twin lamellae. Because the degree of relaxation is random and widespread across the entire population, the original fluid density signature is completely destroyed. This creates a flat, uniform statistical "plateau" of T_h values spanning the entire temperature range between the true formation temperature (T_{form}) and the maximum exposure temperature (T_{exp}).

Appendix C: Modeling of laser-induced alteration

The synthetic data modeling for laser-induced stretching represents the localized structural alteration of fluid inclusions caused by physical bubble nucleation sequences during NA-FIM analysis. This methodology encodes the "inverse shockwave susceptibility" hypothesis, where the primary driver of T_h shifts is the severe geometric concentration of acoustic energy within small micro-cavities. The modeling results are presented in two synchronized graphical formats: inclusion volume versus T_h cross-plots and stacked histograms illustrating the resulting distribution geometries.

The interactive implementation of this model and its visualization parameters are available in the simulation suite (3_laser_alt.py; Dublyansky, 2026a).

https://doi.org/10.5194/egusphere-2026-6315
Preprint. Discussion started: 4 November 2026
© Author(s) 2026. CC BY 4.0 License.

Core concepts governing the modeling framework

The data generation approach for this section is governed by three physical principles that define the behavior of laser-induced mechanical stretching:

1. **Inverse shock susceptibility:** The model assumes that laser shockwave energy density concentrates most destructively within the smallest available cavity volumes. The peak mechanical stress intensity acting at the inclusion-host interface is inversely proportional to the cavity volume. Consequently, small inclusions experience the highest internal pressure spikes and the most severe resulting irreversible volume expansion.
2. **Stochastic, chaotic failure (uncapped stretching):** Laser shock stress alters the inclusion cavity volume by rapid mechanical deformation along cleavage planes or dislocations. Unlike post-depositional thermal re-equilibration, this laser-driven process is purely mechanical and is not bounded by a thermodynamic temperature limit. The resulting upward shifts in T_h are therefore modeled as variable, open-ended, and uncapped by external ambient conditions.
3. **Large inclusions as attenuation sinks:** Large fluid inclusions (10,000–100,000 μm^3) act as robust energy sinks. These wide cavities possess sufficient internal fluid path length to attenuate and damp the laser-induced shockwave before critical yielding stresses can propagate into the surrounding host calcite lattice, thereby preserving the original, pristine formation signal.

Mathematical generation of laser alteration scenarios

To simulate laser alteration across the sample pool, a user-defined percentage of inclusions within each volume class is partitioned into pristine and altered fractions. The pristine fraction is tightly bound by a normal distribution centered at the true baseline formation temperature (T_{form} = 15.0°C, SD = 0.3°C).

For the altered fraction, an upward temperature shift is calculated using a continuous, non-linear function where the expected mean temperature shift and its associated chaotic dispersion decay linearly against the log-transformed volume of each individual inclusion ($\log_{10}(V)$). This mathematically reproduces a continuous negative slope across the inclusion volume versus T_h cross-plots.

Scenario 1: Inverse size-dependent stretching

Mathematical Formulation

The alteration overprint is generated via a continuous log-volume decay function governed by a baseline intensity parameter of 1.8 and a noise spread factor of 0.6.

- **V1 size class (< 1,000 μm^3; Vulnerability Zone):** The altered fraction undergoes severe, open-ended positive skew. Due to the low log-volume values, the continuous function generates the highest upward shifts, resulting in an elevated cluster with an effective mean centered around 21.0°C and wide dispersion (SD = 2.0°C).

https://doi.org/10.5194/egusphere-2026-6315
Preprint. Discussion started: 4 November 2026
© Author(s) 2026. CC BY 4.0 License.

- **V2 size class (1,000 to 10,000 μm³; Transitional Zone):** The altered fraction exhibits a moderate, transitional upward shift governed by the decaying logarithmic function. This results in an intermediate, higher-variance push above the baseline (effective mean centered around = 17.5°C, SD ≈ 1.2°C.
- **V3 size class (10,000 to 100,000 μm³; Stable Anchor Zone):** This class remains unaltered relative to the baseline (effective mean centered around = 15.0°C, SD ≈ 0.3°C).
- **Boundary Constraints:** The overprint intensity tracks a continuous, negative logarithmic slope across the entire volume continuum, naturally tapering off as it approaches the maximum cross-plot limits.

Physical Interpretation

This scenario represents an experimental run where the femtosecond laser's pulse energy is set too high for small-volume inclusion geometries, causing an accidental mechanical overprint during the bubble nucleation attempt.

When the ultra-short pulse is focused into a minute V1 cavity, the concentrated volumetric energy density generates an intense plasma and an acoustic stress wave. Because smaller inclusions have a tiny physical footprint and negligible internal fluid path length to damp the energy, the mechanical shockwave collides directly with the surrounding calcite walls at near-peak intensity. This localized stress irreversibly stretches the soft cleavage planes, lowering the internal fluid density and forcing the subsequently measured T_h values to shift upward past the true 15.0°C baseline. In contrast, large V3 inclusions possess an expansive fluid volume buffer that safely attenuates the shockwave, allowing bubble nucleation to occur without altering the cavity geometry

Scenario 2: Attenuated Pulse (Matrix Preservation)

Mathematical Formulation

The optimized alteration overprint is generated by dampening the continuous log-volume function, utilizing a reduced baseline intensity parameter of 0.4 and a tightly restricted noise spread factor of 0.2.

- **V1 size class (< 1,000 μm³; Vulnerability Zone):** The altered fraction undergoes a highly restricted, low-amplitude upward shift, resulting in a tight cluster with an effective mean centered around 18.5°C (SD ≈ 1.2°C), representing minor, sub-critical cavity stretching.
- **V2 size class (1,000 to 10,000 μm³; Transitional Zone):** The transitional class experiences a negligible thermodynamic shift, plotting as a compact cloud situated immediately above the baseline with an effective mean centered around 15.5°C (SD ≈ 0.4°C).
- **V3 size class (10,000 to 100,000 μm³; Stable Anchor Zone):** The large class remains unaltered and locked at the baseline environmental formation temperature (mean = 15.0°C, SD = 0.3°C), with an exceptionally low stochastic unzipping failure rate of less than 2% centered around 16.5°C.

https://doi.org/10.5194/egusphere-2026-6315
Preprint. Discussion started: 4 November 2026
© Author(s) 2026. CC BY 4.0 License.

- **Boundary Constraints:** The alteration overprint decays rapidly across the volume continuum, preserving the original environmental characteristics across more than 80% of the collective sample pool.

Physical Interpretation

This scenario models a perfectly optimized, low-fluence femtosecond laser protocol, the gold standard for nucleation-assisted microthermometry in speleothem research.

By utilizing an expertly attenuated laser beam, the single pulse delivers exactly enough transient mechanical energy to overcome the kinetic barrier to phase separation and nucleate the missing shrinkage bubble, safely stopping short of breaching the calcite host's structural yield threshold. The minimal mechanical overprint is strictly restricted to the highest-curvature margins of the smallest V1 inclusions, which register only negligible volume changes. The rest of the fluid inclusion assemblage across the V2 and V3 size classes undergoes bubble nucleation with zero geometric deformation. This demonstrates an analytically flawless experimental run that perfectly preserves the pristine environmental formation signal of the speleothem.

Code availability

The software utilized for the physics-informed modeling presented in the figures of this manuscript is archived at Zenodo (Dublyansky, 2026a). The computational tool for evaluating measured data and calculating the proposed statistical metrics (Q1 and 95% CI) is also archived at Zenodo (Dublyansky, 2026b).

Author contributions

YD designed the study, conducted the numerical modeling, developed the accompanying software, and wrote the manuscript.

Competing interests

The author declares no competing interests.

https://doi.org/10.5194/egusphere-2026-6315
Preprint. Discussion started: 4 November 2026
© Author(s) 2026. CC BY 4.0 License.

Disclaimer

Copernicus Publications remains neutral with regard to jurisdictional claims made in the text, published maps, institutional affiliations, or any other geographical representation in this paper. While Copernicus Publications makes every effort to include appropriate place names, the final responsibility lies with the authors. Views expressed in the text are those of the authors and do not necessarily reflect the views of the publisher.

Acknowledgements

The author is grateful for the hospitality and practical research experience gained at the Fluid Inclusion Laboratory within the Department of Earth Sciences at the University of Bergen, Norway. Insightful and fruitful discussions with members of the Bergen FluidMICS group—including Y. Krüger, L. Pasqualetto, J. Maccali, and N. Meckler—are gratefully acknowledged. During the preparation of this work, an AI language model was utilized to assist with Python programming and to improve the readability and linguistic flow of the manuscript. The author reviewed, edited, and validated all text and code generated by this tool, and assumes full responsibility for the final publication.

Financial support

This research was funded in part by the Austrian Science Fund (FWF) grant 10.55776/P36416. For open access purposes, the author has applied a CC BY public copyright license to any author accepted manuscript version arising from this submission.

References

Anderson, T. L.: Fracture Mechanics: Fundamentals and Applications, 4th edn., CRC Press, 2017.

Arnuk, W. D., Guillerm, E., Lowenstein, T. K., Krüger, Y., Olson, K. J., Lensky, N. G., and Brauer, V.: Nucleation-assisted microthermometry: A novel application to fluid inclusions in halite, Chem. Geol., 667, 122318, https://doi.org/10.1016/j.chemgeo.2024.122318, 2024.

Chemin, A., Fawaz, M. W., and Amans, D.: Investigation of the blast pressure following laser ablation at a solid–fluid interface using shock waves dynamics in air and in water, Appl. Surf. Sci., 574, 151592, https://doi.org/10.1016/j.apsusc.2021.151592, 2022.

https://doi.org/10.5194/egusphere-2026-6315
Preprint. Discussion started: 4 November 2026
© Author(s) 2026. CC BY 4.0 License.

Domínguez-Villar, D., Lojen, S., Krklec, K., Baker, A., and Fairchild, I. J.: Is global warming affecting cave temperatures? Experimental and model data from a paradigmatic case study, Clim. Dynam., 45, 569–581, https://doi.org/10.1007/s00382-014-2226-1, 2014.

Dublyansky, Y.: Interactive Modeling Suite for Post-Entrapment Fluid Inclusion Alteration [code], Zenodo, https://doi.org/10.5281/zenodo.23285702, 2026a.

Dublyansky, Y.: Nucleation-Assisted Fluid Inclusion Microthermometry (NA-FIM) Analyzer: A Tool for Speleothems and Low-Temperature Minerals [code], Zenodo, https://doi.org/10.5281/zenodo.23279977, 2026b.

Dublyansky, Y., Ford, D., and Reutski, V.: Traces of epigenetic hydrothermal activity at Yucca Mountain, Nevada: preliminary data on the fluid inclusion and stable isotope evidence, Chem. Geol., 173, 125–149, https://doi.org/10.1016/S0009-2541(00)00271-0, 2001.

Frisia, S., Borsato, A., Fairchild, I. J., and McDermott, F.: Calcite fabrics, growth mechanisms, and environment of formation in speleothems from the Italian Alps and southwestern Ireland, J. Sediment. Res., 70, 1183–1196, https://doi.org/10.1306/022900701183, 2000.

Goldstein, R. H. and Reynolds, T. J.: Systematics of Fluid Inclusions in Diagenetic Minerals, SEPM (Society for Sedimentary Geology), Tulsa, OK, 1994.

Griffith, A. A.: The phenomena of rupture and flow in solids, Philos. T. R. Soc. A, 221, 163–198, https://doi.org/10.1098/rsta.1921.0006, 1921.

Koltai, G., Kluge, T., Krüger, Y., Spötl, C., Rinyu, L., Audra, P., Honiat, C., Leél-Őssy, S., and Dublyansky, Y.: Geothermometry of calcite spar at 10–50°C, Sci. Rep., 14, 1553, https://doi.org/10.1038/s41598-024-51937-4, 2024.

Krüger, Y., Marti, D., Staub, R. H., Fleitmann, D., and Frenz, M.: Liquid–vapour homogenisation of fluid inclusions in stalagmites: Evaluation of a new thermometer for palaeoclimate research, Chem. Geol., 289, 39–47, https://doi.org/10.1016/j.chemgeo.2011.07.009, 2011.

Krüger, Y., Pasqualetto, L., Fernandez, A., Cobb, K. M., and Meckler, A. N.: Tropical temperature evolution across two glacial cycles derived from speleothem fluid inclusion microthermometry, Clim. Past, 21, 1553–1584, https://doi.org/10.5194/cp-21-1553-2025, 2025.

Krüger, Y., Stoller, P., Rička, J., and Frenz, M.: Femtosecond lasers in fluid-inclusion analysis: overcoming metastable phase states, Eur. J. Mineral., 19, 693–706, https://doi.org/10.1127/0935-1221/2007/0019-1762, 2007.

Linz, N., Freidank, S., Liang, X.-X., and Vogel, A.: Laser-induced plasma formation and cavitation in water: from nanoeffects to extreme states of matter, Rep. Prog. Phys., 88, https://doi.org/10.1088/1361-6633/adedb3, 2025.

Løland, M. H., Krüger, Y., Fernandez, A., Buckingham, F., Carolin, S. A., Sodemann, H., Adkins, J. F., Cobb, K. M., and Meckler, A. N.: Evolution of tropical land temperature across the last glacial termination, Nat. Commun., 13, 5158, https://doi.org/10.1038/s41467-022-32712-3, 2022.

https://doi.org/10.5194/egusphere-2026-6315
Preprint. Discussion started: 4 November 2026
© Author(s) 2026. CC BY 4.0 License.

Maccali, J., Meckler, A. N., Lauritzen, S.-E., Brekken, T., Rokkan, H. A., Fernandez, A., Krüger, Y., Adigun, J., Affolter, S., and Leuenberger, M.: Multi-proxy speleothem-based reconstruction of mid-MIS 3 climate in South Africa, Clim. Past, 19, 1847–1862, https://doi.org/10.5194/cp-19-1847-2023, 2023.

Marti, D., Krüger, Y., Fleitmann, D., Frenz, M., and Rička, J.: The effect of surface tension on liquid-gas equilibria in isochoric systems and its application to fluid inclusions, Fluid Phase Equilibr., 314, 13–21, https://doi.org/10.1016/j.fluid.2011.08.010, 2012.

Meckler, A. N., Affolter, S., Dublyansky, Y. V., Krüger, Y., Vogel, N., Bernasconi, S. M., Frenz, M., Kipfer, R., Leuenberger, M., Spötl, C., Carolin, S., Cobb, K. M., Moerman, J., Adkins, J. F., and Fleitmann, D.: Glacial–interglacial temperature change in the tropical West Pacific: A comparison of stalagmite-based paleothermometers, Quaternary Sci. Rev., 127, 90–116, https://doi.org/10.1016/j.quascirev.2015.06.015, 2015.

Murthy, D. N. P., Xie, M., and Jiang, R.: Weibull Models, John Wiley & Sons, https://doi.org/10.1002/047172106X, 2004.

Noack, J. and Vogel, A.: Streak-photographic investigation of shock wave emission after laser-induced plasma formation in water, Proc. SPIE, 2391, 284–293, https://doi.org/10.1117/12.209894, 1995.

Pahl, B. L., Meckler, A. N., Krüger, Y., Wright, K. T., Serrato Marks, G., Jost, A. B., McGee, D., Wanamaker, A. D., Ankerstjerne, S., and Johnson, K. R.: Terrestrial Temperature Variability and Its Impact on Vegetation and Moisture Dynamics During Dansgaard-Oeschger Event 22 in Northern Mexico, Geophys. Res. Lett., 52, e2025GL117169, https://doi.org/10.1029/2025GL117169, 2025.

Pasqualetto, L., Mekler, N., and Krüger, Y.: FluidMICSolver: a standalone application for nucleation-assisted microthermometry of fluid inclusions in speleothems, in preparation.

Roedder, E.: Fluid Inclusions, Reviews in Mineralogy, vol. 12, Mineralogical Society of America, Chantilly, VA, 1984.

Spadin, F., Marti, D., Hidalgo-Staub, R., Rička, J., Fleitmann, D., and Frenz, M.: Technical Note: How accurate can stalagmite formation temperatures be determined using vapour bubble radius measurements in fluid inclusions?, Clim. Past, 11, 905–913, https://doi.org/10.5194/cp-11-905-2015, 2015.

Vogel, A., Noack, J., Hüttman, G., and Paltauf, G.: Mechanisms of femtosecond laser nanosurgery of cells and tissues, Appl. Phys. B, 81, 1015–1047, https://doi.org/10.1007/s00340-005-2036-6, 2005.

Weibull, W.: A statistical theory of the strength of materials, Ingeniörs Vetenskaps Akademien Handlingar (Proceedings of the Royal Swedish Institute for Engineering Research), No. 151, 1939.

Wilson, N. S. F., Cline, J. S., and Amelin, Y. V.: Origin, timing, and temperature of secondary calcite–silica mineral formation at Yucca Mountain, Nevada, Geochim. Cosmochim. Acta, 67, 1145–1184, https://doi.org/10.1016/S0016-7037(02)01205-X, 2003.